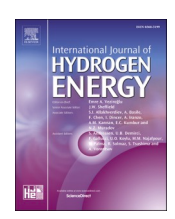
ELSEVIER

Contents lists available at ScienceDirect

# International Journal of Hydrogen Energy

journal homepage: www.elsevier.com/locate/he





# Underwater release of hydrogen-natural gas blends

J.E. Olsen \* D, P. Skjetne

SINTEF, 7465 Trondheim, Norway

#### ARTICLE INFO

Handling Editor: Ramazan Solmaz

Keywords: Underwater gas release Safety risk numerical model CFD

#### ABSTRACT

The transport of hydrogen and hydrogen-natural gas blends through subsea pipelines introduces significant safety risks in the event of pipeline damage or rupture. Such incidents can lead to the release of gas, forming a bubble plume that ascends to the ocean surface. Elevated surface concentrations of hydrogen and hydrogen-natural gas may pose serious hazards to life and infrastructure. Risk assessments typically involve a sequence of analyses, with gas migration and dissolution in the water column representing a source of uncertainty. This study presents a transient, three-dimensional computational fluid dynamics model developed to quantify the surfacing gas volume, its composition, and spatio-temporal distribution for a multicomponent gas. The model aims to improve the accuracy of quantitative risk assessment related to subsea hydrogen transport. The model is applied to underwater release scenarios with varying hydrogen content and model results demonstrate that the risk increases with increasing hydrogen content.

# 1. Introduction

Hydrogen is an attractive energy carrier for the green transition. The distribution of hydrogen through pipelines is partly envisaged in existing infrastructure for natural gas. This might save costs but has a negative impact on material integrity due to steel embrittlement and more. A compromise is to transport a blend of hydrogen and natural gas [1,2]. While this reduces the risk of failure due to material degradation, leaks and pipeline ruptures may still occur due to external factors. This can potentially result in fatal incidents related to hydrogen's flammability, explosiveness and asphyxiation characteristics. Hydrogen has been the cause of many incidents and fatalities, and most of these are related to piping and pipelines [3].

The large-scale production of hydrogen will require corresponding large-scale transport solutions, likely including the use of subsea pipelines for parts of the distribution network. If a pipeline is damaged such that a hole, crack or full bore opening releases gas, the gas will rise to the surface due to buoyancy. At substantial release rates, the gas ascends as a bubble plume, undergoing dispersion and dissolution in the water column. Upon reaching the atmosphere, it is subject to wind-driven dispersion. This process is illustrated in Fig. 1. The resulting atmospheric concentration of hydrogen—or a hydrogen-natural gas blend—determines the associated risk potential.

Assessing safety and risks associated with underwater release of hydrogen or hydrogen blends rely on quantitative input from several

analysis. This includes predictions on how the gas migrates and dissolves in the ocean before it reaches the surface and how the gas is dispersed into the atmosphere. This has historically been studied for release of methane and natural gas in relation to risks in natural gas extraction and export. While methane has a flammability range limited to a concentration of 5–15 % in air, hydrogen can sustain combustion at a wider range between 4 % and 75 % [4]. Hydrogen has also a wider explosive range, lower ignition energy and faster flame propagation. The risk potential in most scenarios is thus higher for hydrogen.

Early work on dispersion of large scale underwater bubble plumes is often credited to Taylor in 1955 [5], even if some work date back to 1937 [6]. Batchelor [7], Evans [8] and Morton et al. [9] also published studies around the same time. These early studies applied so-called integral models which assumes a profile, either Gaussian or top-hat, for the velocity and bubble volume fraction which widens according to the entrainment hypothesis. The model was later enhanced by Ditmars and Cederwall [10] by including gas compressibility and bubble slip velocity. The focus of these early modelling attempts was on use of bubble plumes as breakwaters. Later the focus has shifted towards underwater release of oil and gas. Topham [11] published the first study on underwater oil release and Fanneløp & Sjøen [12] and Milgram [13] on underwater gas release. The integral concept was further refined by several scientists including Yapa and Zhen (1997) [14], Socolofsy & Adams (2002) [15] and Johansen (2003) [16]. The pioneering integral models were developed in an era with limited computational

E-mail address: jan.e.olsen@sintef.no (J.E. Olsen).

<sup>\*</sup> Corresponding author.

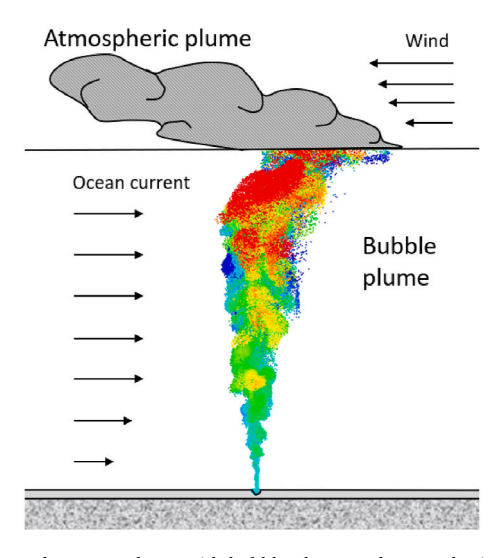


Fig. 1. Underwater release with bubble plume and atmospheric plume.

capabilities and did not include high levels of complexity. The more recently developed models allow for calculations of transient 3-dimensional plumes with multicomponent gas bubbles and oil droplets in complex oceanographic conditions exposed to gas dissolution and stripping, e.g. Dissanayake et al. (2018) [17].

The advancement of numerical computing and computational fluid dynamics (CFD) enabled more resolved mathematical models. Buscaglia et al. [18] developed an Eulerian-Eulerian axisymmetric 2-dimensional model to study aeration of lakes. It was applied to very small release rates (<0.001 kg/s) and the 2D-approach allowed for a high resolution. A model for transient 3-dimensional ocean bubble plumes capable of assessing realistic release rates from pipeline rupture was first developed by Cloete et al. (2009) [19]. A major challenge for CFD is the large scale difference between bubbles, nozzle diameter (release diameter) and ocean depth. While an Eulerian-Eulerian approach will suffice when replicating a small scale lab experiment (depth  $\leq 1$  m) [20], Cloete et al. [19] applied an Eulerian-Lagrangian model and validated the model against an experiment in a 7 m deep water pool [21] since the Eulerian-Eulerian approach did not reproduce observations at affordable resolutions at the time (2009). The Eulerian-Lagrangian model has more recently been enhanced to include a transient VLES-turbulence model and gas dissolution by Olsen & Skjetne [22]. Several others have also adopted CFD to study underwater gas plumes, including Fraga et al. who developed a modelling concept with an LES-turbulence model [23] and the COEST-centre (Li and Chen) [20,24] who also conducts small scale lab experiments. More recently Cassano et al. developed a CFD model incorporating pipeline, water column and atmosphere in one simulation [25]. Due to different time scales in the various parts of the domain, only a 2-dimensional model could be applied due to the high computational cost.

The study of underwater gas plumes has also been addressed by a series of experiments, most of which are at small scales (depth  $\lesssim 1$  m) and with air, e.g. Refs. [15,20]. At larger scales Milgram conducted experiments in a sinkhole at Bugg Spring from a depth of 50 m with release rates of air up to 0.71 kg/s [13] and Engebretsen released air with rates ranging from 0.10 to 0.92 kg/s in a 7 m deep pool. Experiments in the ocean has also been performed, including the DeepSpill experiment at 844 m by Johansen et al. [26]. The DeepSpill experiment primarily focused on oil release, but also released natural gas at 0.6 and 0.7 Nm³/s. These and other experiments are discussed by Olsen & Skjetne [27]. When focusing on safety, the releases of interest are those of higher intensity since the weaker releases do not *per se* pose any safety issue. Such conditions can be reproduced in the lab at small scale, but at large scale very few experiments have been conducted. At significant

ocean depths a controlled release from 130 m of 17 kg/s of natural gas was monitored in relation to an offshore pigging operation [22]. Apart from that there are some observations on incidents, including the more recent Nord Stream incident [28,29]. In addition a series of experiments have been conducted on single bubbles and natural seeps to establish reliable models for the gas dissolution and the mass transfer coefficient, e.g. Refs. [30–34].

When assessing safety risks, the surface flux of gas and its transient behaviour is a vital output from underwater bubble plume model. While the plume is well described by a Gaussian or top-hat profile in the water column, that is not the case for the surface flux [35]. Still, Mercuri et al. [36] got results on CO2 plumes with an integral model which did not deviate significantly from time-averaged CFD results. However, turbulence dictates some transient local peaks of surface flux which is important for an assessment since maximum values can trigger ignition and be the values triggering sensors. This is inherently captured by CFD models with a transient turbulence model (e.g. LES or VLES). CFD models also capture surface waves and outwelling flow from the surfacing plume which are important for assessing hydrodynamic loads on surface vessels. Due to this the authors chose to apply a CFD model in their study on safety related to underwater release of gas. The model has previously been applied to single component gas release of either methane, carbon dioxide or air.

For pure hydrogen transport, existing models for methane and natural gas can be applied by replacing material properties for methane with hydrogen. To the authors knowledge, only Li et al. [24] have studied underwater release of hydrogen. This is, however, at a lab scale where dissolution have minimal impact. Mercuri et al. [36] discusses hydrogen releases, but do not present any results. However, many plans for hydrogen transport are based on using existing infrastructure for natural gas. As mentioned above, these pipelines are envisaged to transport a blend of hydrogen and natural gas. This necessitates mathematical models accounting for gas bubbles consisting of multiple species. If that capability is in place, it will also be worthwhile to account for stripping of oxygen and nitrogen from the ocean to the bubbles. Oxygen and nitrogen are present in the ocean due its large interface with the atmosphere and biological processes producing nitrogen. This can potentially affect the composition of the bubbles entering the atmosphere.

To address the abovementioned challenge a mathematical modelling framework for safety assessment of underwater gas releases based on CFD [22] has been modified from tracking single component gas to tracking multicomponent gas bubbles. This has previously not been addressed by any CFD models for underwater gas release. Material properties of hydrogen, nitrogen and oxygen have been added to the framework which is been applied to study the fate of underwater release of hydrogen blends. While Liu et al. [37] discusses leaks from pipeline transport of hydrogen blends, their main focus is on onshore buried pipelines and only addresses results on pure methane for subsea pipelines. The study presented here is therefore a first of its kind concerning large scale bubble plumes from underwater release of hydrogen blends and its implication on safety.

While the focus of this study is on the dispersion and dissolution of gas in the water column and how the gas surfaces into the atmosphere, it is important to note that the overall quantitative risk assessment (QRA) also includes analysis to e.g. quantify the gas release rate and the dispersion of gas in the atmosphere. Dispersion of gas in the atmosphere determines the extent of the safety zone (exclusion zone, stand-off distance). For the atmospheric dispersion analysis the surface flux of gas as predicted by the model for the water column presented in this study is a governing input together with wind profiles [38,39].

## 2. Mathematical modelling framework

Conservation of mass, momentum and energy governs the evolution of composition, motion and temperature of bubbles and nearby ocean waters. This is expressed mathematically by conservation laws. Here we apply an Eulerian-Lagrangian CFD model developed by Cloete et al. [19] and enhanced by Olsen & Skjetne [22] including gas dissolution and a VLES turbulence model. The velocities, temperature and concentration of dissolved species in the ocean (and the atmosphere above) are calculated in the Eulerian framework with a Geo-reconstruct scheme to track the interface between ocean and atmosphere [22]. The bubbles are tracked in a Lagrangian framework in which Newton's second law provides a force balance on the bubbles. This is mathematically expressed by

$$\frac{d\overrightarrow{u}_{b}}{dt} = \frac{\overrightarrow{g}(\rho_{b} - \rho_{w})}{\rho_{b}} + \overrightarrow{F}_{D} + \overrightarrow{F}_{VM}$$
 Eq.(1)

Here  $\overrightarrow{u}_b$  is bubble velocity,  $\overrightarrow{g}$  is gravity,  $\rho_b$  is bubble density,  $\rho_w$  is local sea water density, and  $\overrightarrow{F}_D$  and  $\overrightarrow{F}_{VM}$  represent drag force and virtual mass force. The first term on the right-hand side represents buoyancy. The drag force between bubbles and ocean water is given by

$$\overrightarrow{F}_D = \frac{18\mu}{\rho_b d_b^2} \frac{C_D \text{Re}}{24} \left( \overrightarrow{u}_w - \overrightarrow{u}_b \right)$$
 Eq.(2)

where  $C_D$  is drag coefficient, Re is Reynolds number,  $d_b$  is bubble diameter and  $u_w$  is local velocity of ocean water. Since the drag force includes a velocity difference between bubble velocity and local ocean velocity, the bubble motion is coupled to the ocean velocity. The ocean velocity is also governed by conservation of momentum. This is mathematically expressed in an Eulerian framework by the Navier-Stokes equation also including a drag term coupling back to the bubble velocity. This ensures a two-way coupling between bubbles and ocean water. Further details, including turbulence model and bubble size are given by Olsen & Skjetne [22].

Energy is also exchanged between bubbles and ocean since bubbles might be released at a different temperature than the temperature of the ocean water. This is calculated by equations conserving energy for bubbles and ocean water resulting in a temperature field. The temperature field affects material properties important to motion and mass transfer. For a Langrangain bubble, energy conservation is expressed by

$$m_b c_b \frac{dT_b}{dt} = \pi d_b^2 h_b (T_w - T_b) + S_s$$
 Eq.(3)

Here  $m_b$  is the mass of the bubble,  $c_b$  is the heat capacity of the bubble,  $T_b$  and  $T_w$  is the temperature of the bubble and the surrounding water,  $d_b$  is the bubble diameter and  $h_b$  is the heat transfer coefficient.  $S_s$  is the source term for heat of solution [17].

Mass transfer or gas dissolution is driven by the ocean's ability to dissolve gas species. For many relevant gas components gas dissolution in water is significant. The earlier versions of this framework only accounted for a single gas component. Assessment of multicomponent gases thus requires an enhanced mathematical framework. Mass transfer from a gas bubble to the surrounding ocean is limited by the diffusion and convection of species on the liquid side of the interface. The mass transfer rate  $\dot{m_i}$  of species i, can be expressed by the Ranz-Marshall equation [40]

$$\dot{m}_i = \pi d_b^2 \ k_i \left( c_i^{sol} - c_i^w \right)$$
 Eq.(4)

Here  $k_i$  is the mass transfer coefficient,  $c_i^{sol}$  is solubility of species i in the ocean and  $c_i^w$  is the local concentration of the species in the ocean. If the bubble consists of multiple species of gas it is important to apply the partial pressure  $p_i$  of the species in question when extracting the solubility

$$c_i^{sol} = c_i^{sol}(p_i, T)$$
 Eq.(5)

It is assumed that the fugacity coefficient of a species in a mixture is equivalent to that of the species by itself. The partial pressure is given by

the molar fraction  $x_i$  or the mass fraction  $Y_i$  of species i in the gas bubble

$$p_i = x_i P = \frac{Y_i / M_i}{\sum Y_k / M_k} P$$
 Eq.(6)

where P is local total pressure and  $M_i$  is the molar weight of species i. The generalisation to a multicomponent gas is primarily given by the use of partial pressure instead of total pressure in Eq. (4). In addition, the updated mass of a bubble now involves a sum of the contribution from all species expressed by

$$m_{i,j} = m_{i,j-1} + d\dot{t} \cdot m_{i,j-1}$$
 Eq.(7)

where j indicates timestep number and dt indicates the numerical timestep. The total mass of a bubble is the sum of the mass of each species within the bubble

$$m_j = \sum_i m_{i,j}$$
 Eq.(8)

At the end of each timestep the molar fractions are updated according to

$$x_{i,j} = \frac{m_{i,j}/M_i}{\sum m_{i,j,k}/M_k}$$
 Eq.(9)

It should be noted that a modification of the code architecture is needed when tracking n species instead of one. This also adds a substantial larger set of material properties.

#### 2.1. Material properties

Gas properties which affect the fate of the bubble plume are primarily density, solubility and diffusivity. Gas viscosity has a smaller impact on bubble size in bubbly flows of high turbulence intensity and is given by Wilke's equation [41] for a gas mixture. The density of the gas species involved directly affects the buoyancy of the gas. It is currently assumed to be represented by an ideal gas. In reality this assumption is not adequate for higher pressures typically at depths of 300 m and deeper as seen in Fig. 2. At 500 m the deviation from real gas data from NIST (National Institute of Standards and Technology) [42,43] on CH<sub>4</sub> is about 10 % [27]. For this comparative study, the assumption of an ideal gas is acceptable. The density of the multicomponent gas (gas mixture) is the sum of all gas species weighted by their molar fraction

$$\rho = \sum_{i} x_{i} \rho_{i} = \sum_{i} \frac{x_{i} P M_{i}}{RT}$$
 Eq.(9)

Here the assumption of ideal gas is seen in the last expression. This will be modified to account for real gases in future work.

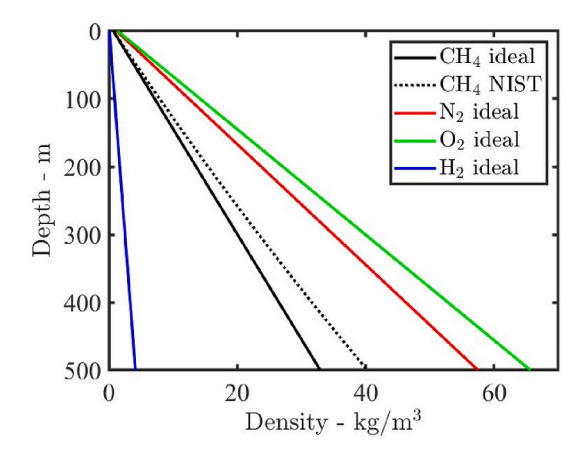


Fig. 2. Gas density as function of depth at 5  $^{\circ}\text{C}$  for ideal gas and proper data from NIST for CH<sub>4</sub>.

As seen from Eq. (3), solubility governs how much of the released gas can be dissolved in the ocean. It varies with temperature, pressure and salinity. For hydrogen and methane we apply the correlations derived by Wiesenburg & Guinasso [44]. For nitrogen and oxygen we apply the correlations for pure water (freshwater) from Perry's handbook [4] corrected for salinity according to Hamme & Emerson [45] and Garcia & Gordon [46] for nitrogen and oxygen, respectively. Plots of solubility as functions of ocean depth (i.e. pressure) is seen in Fig. 3. Methane has the highest solubility and hydrogen the lowest of the four species. Solubility decreases with increasing salinity and temperature. It increases with pressure i.e., ocean depth.

Diffusivity affects the transport of species away from the bubble interface. The mass transfer coefficient which is part of Eq. (3) is a function of the diffusivity of the species in focus. The correlation for diffusivity favoured by Hayduk & Laudie [47] is applied. This was derived by Othmer & Thakar [48] and revised to

$$D_i = \frac{13.26 \cdot 10^{-5}}{\mu_w^{1.4} V_i^{0.589}}$$
 Eq.(10)

where  $D_i$  is the diffusivity (cm<sup>2</sup>/s) of species i,  $\mu_w$  is the viscosity (cP) of the sea water and  $V_i$  is the molar volume of the species.

## 2.2. Model implementation

The mathematical model is implemented as a library of *user-defined-functions* specially developed to capture the governing physics outlined above and in the work of Olsen & Skjetne [22]. This library is linked to the commercial CFD code ANSYS/Fluent which handles the numerical methods and model simulations. In ANSYS/Fluent a VOF (volume of fluid) method is applied to track the interface between ocean and atmosphere, tracking of multiple species is activated and the energy equation is enabled to solve for temperature. As mentioned above, this is coupled to parcel based tracking of bubbles.

The library of *user-defined-functions* includes macros for drag, mass transfer, turbulence, bubble size and removal of bubbles entering the atmosphere. Functions for material properties are also an integral part of the library. All details implemented in these libraries are documented above and/or in previously published work [22].

# 2.3. Model validation

For a mathematical framework to be applied to quantitative risk assessment (QRA), it is critical that the framework is trustworthy. This is done by validating model results with relevant observations. While many experiments have been performed, most of these are in a lab with small scales or in the ocean with very small release rates [27]. Some of these experiments are more relevant than others and the preceding version of the modelling framework has been compared against the observations in these experiments and shown to be consistent [22]. The

updated version documented above has been compared to observations of a controlled 17 kg/s of natural gas release from a depth of 138 m through a valve with an effective opening of 1 inch. This release was linked to a pigging operation for which a release permit was obtained to conduct a field experiment.

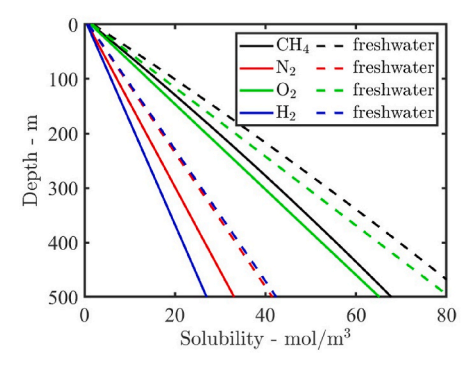
By using this scenario as a validation case and a test on how gas composition affects the behaviour, a series of case studies was conducted. When comparing different gas compositions, it is also important to define how the release rate is specified. This could involve using a consistent total mass flow rate or a consistent volumetric flow rate across all scenarios. Here we have chosen to keep the pipeline operating conditions similar for all scenarios since the study is motivated by safety if hydrogen and hydrogen blends are transported in existing pipelines for natural gas. These are then assumed to be transported under the same conditions as methane (natural gas) with the same pipeline dimensions and same pipeline pressure. With a pipeline pressure of 160 bara and a release valve with an opening of 1 inch, the release conditions are as listed in Table 1. The release rate varies with hydrogen fraction in the gas blend. Due to the narrow release valve, the release rate is dictated by release area, compressibility and the speed of sound of the gas mixture, i. e. choked flow.

These scenarios were assessed by running numerical simulations with the model described abovein a computational domain of 276 x 276  $\times$  193 m with a mesh of 1.5 M cells according to the protocol given by Olsen & Skjetne [22]. Some of the results are seen in Figs. 4 and 5. Fig. 4 shows how fast the front of the plume travels towards the surface. The resulting rise times are listed in Table 1. Rise time is the time it takes for the front of the initial plume to reach the surface after initiation of the release. It is seen that gas composition affects the rise time of the plume. Hydrogen is lighter than methane. This makes hydrogen more buoyant. There is also a distinct difference between a blend of 50 % mol  $\rm H_2$  and 50 % mass  $\rm H_2$ . Thus, it is important to standardise how the gas blending or gas composition is defined. This is illustrated by Fig. 5. The molar-based definition is used for the remainder of the document.

It also seems that the model is consistent with the observed evolution of the plume front. This provides some validation for the model. The earlier version of the model has also been tested against several other

**Table 1**Release rates and conditions for test pipe.

Hydrogen content		Release Volumetric density release rate		Mass release rate	Rise time	
Molar fraction	Mass fraction	kg/m <sup>3</sup>	m <sup>3</sup> /s	kg/s	s	
0.00	0.00	10.4	1.64	17.00	91.0	
0.50	0.11	5.9	3.21	18.77	77.2	
0.89	0.50	2.3	4.44	10.26	69.3	
1.00	1.00	1.3	4.79	6.22	65.8	



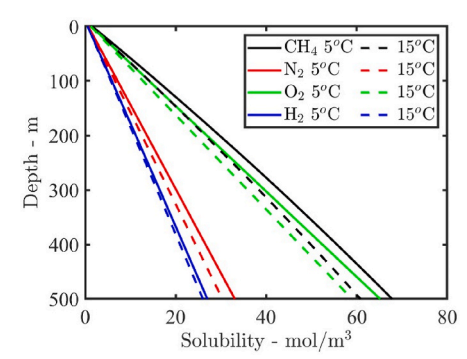
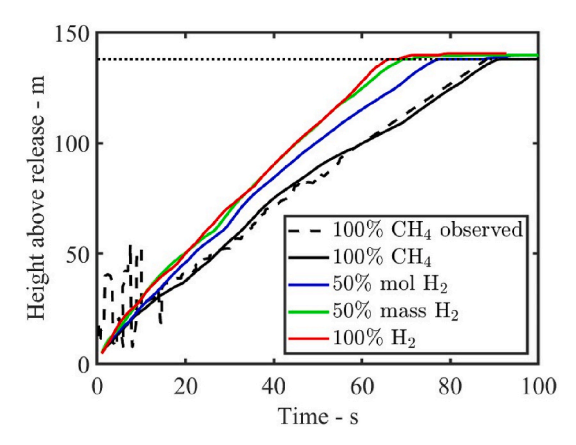
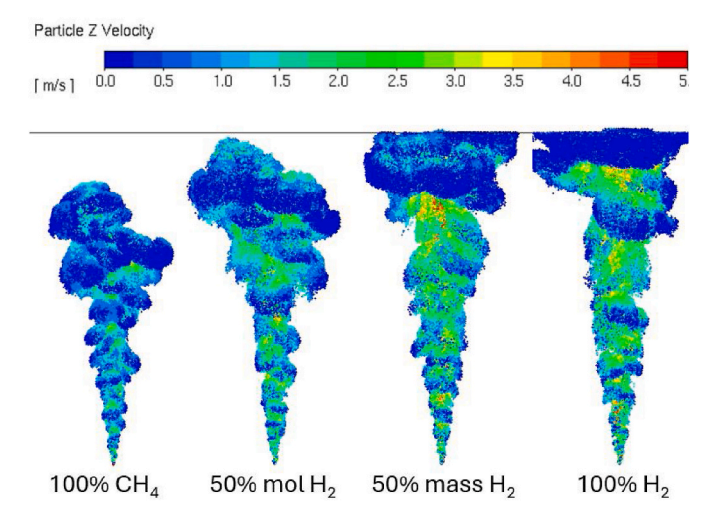


Fig. 3. Solubility for CH<sub>4</sub>, N<sub>2</sub>, O<sub>2</sub> and H<sub>2</sub> as function of depth at 5 °C for a salinity of 30 PSU. Left plot compares with freshwater values. Right plot compares with higher ocean temperature.



**Fig. 4.** Model predictions of plume rise as function of time for various gas blends compared to observations on a release of CH4.



**Fig. 5.** Bubble plumes for various gas blends 75 s after initiation of release coloured by bubble vertical velocity.

observations and experiments with air and methane [22] and shown to be reliable. No relevant experiments have been performed with hydrogen or hydrogen blends to the authors knowledge. Ideally the model should be compared against such experiments.

# 3. Case study on export line

The modelling framework described above can be applied to assess realistic release scenarios. Again, we focus on comparing releases of different gas blends based on similar pipeline operating conditions. The reference is a pipeline releasing 300 kg/s of methane from 300 m in a typical export pipe with a 4-inch release area, e.g., from a faulty subsea valve or resulting from an unintended impact. This is not an initial release rate but is representative for a typical release rate when the

pressure in the pipeline is around 100 bara and possible interventions may be underway. The calculated release scenarios are seen in Table 2. The trend is that the mass rate decreases with increasing hydrogen content and the volumetric rate increases. The higher heating value (HHV) is the upper limit of the available thermal energy output by complete combustion. This is higher for hydrogen (141.8 MJ/kg) than methane (55.5 MJ/kg). Due to the higher value for hydrogen, the HHV of the release varies little even if the total release rate decreases with increasing hydrogen content.

Numerical simulations on the scenarios were performed in a 600 x  $600 \times 420$  m computational domain with a mesh of 1.5 M cells. The resulting plumes are depicted in Fig. 6. Qualitatively it seems like more hydrogen content promotes a stronger and more buoyant plume. This is confirmed by the buoyancy flux of the releases as listed in Table 2. Fig. 7 show plots of time-varying surfacing rates and HHV at the surface for all scenarios. The surfacing rates is the mass rate of gas reaching the surface. Fig. 7 a) represents the scenarios with either pure CH<sub>4</sub> (100 % mol CH<sub>4</sub>) or pure H<sub>2</sub> (100 % mol H<sub>2</sub>) releases. The release with 100 % mol H<sub>2</sub> surfaces 87 s after initiation of the release which is shorter than that of a pure CH<sub>4</sub> release which surfaces after 140 s. This is explained by the higher buoyancy of H<sub>2</sub> in comparison to CH<sub>4</sub>. Due to turbulence the surfacing rates fluctuate. At an equivalent release rate, methane dissolves more in the ocean than hydrogen. 58 % of CH<sub>4</sub> is dissolved compared to 20 % of H<sub>2</sub> (average of surfacing rate for the last 300 s of observation). This is caused by the higher solubility of CH<sub>4</sub> compared to

The surfacing rate for the scenario where a small fraction of H<sub>2</sub> (4 % mol) is added to the CH<sub>4</sub> stream is plotted in Fig. 7 b). Due to the low hydrogen content, the hydrogen surfacing rate is plotted against a second y-axis with a different scale. The release surfaces after 121 s and 55 % of the gas is dissolved in the ocean. This deviates almost insignificantly from the release of pure CH<sub>4</sub>. For the release of 50 % mol H<sub>2</sub>, the surfacing rate is seen in Fig. 7 c). The release surfaces after 129 s and 44 % of the released gas is dissolved. The gas dissolution is 46 % for CH<sub>4</sub> and 26 % for H2 indicating that the bubbles changes composition as they rise to the surface and thus obtaining a higher concentration of H<sub>2</sub> at the surface. Initial release rate, initial gas composition and gas dissolution dictates the surfacing rate and the surfacing composition. This is reflected by the higher heating value of the surfacing gas. This is plotted in Fig. 7 d). Even if the release rate decreases with increasing H<sub>2</sub> content, the HHV increases with increasing H<sub>2</sub> content due to the higher heating value of H<sub>2</sub> compared to CH<sub>4</sub>. Time averaged values of these results are listed in Table 2.

Due to drag forces and momentum transfer between gas bubbles and surrounding ocean water, water is moved upwards in the plume. At the surface this water is pushed outwards, causing radial surface flow from the centre of the plume and waves. The time averaged maximum value of the this surface velocity is also given in the table This indicates the agitation at the ocean surface caused by the gas release. It will impose forces on surface vessels and infrastructure which will be perceived as hydrodynamic loads. This is an additional risk which needs to be assessed. An increase in hydrogen content increases the surface velocity and hydrodynamic loads. This is attributed to hydrogen being more buoyant than methane as indicated by the buoyancy flux of the releases

 Table 2

 Release rates, conditions for pipeline rupture and surfacing results.

Hydroge content	en	Release density	Volumetric release rate	Mass release rate	Buoyancy release flux	Release HHV	Rise time	Surface flux	Dis- solution	Top HHV	Surface velocity
% mol	% kg	kg/m <sup>3</sup>	m <sup>3</sup> /s	kg/s	$m^3/s^4$	GJ/s	s	kg/s	%	GJ/s	m/s
0.0	0.00	21.7	13.8	300.0	6279	16.65	139.8	127.4	57.6	7.05	4.74
4.0	0.01	21.0	14.0	294.7	6628	16.49	120.7	134.2	54.6	7.53	4.76
50.0	0.11	12.2	18.4	225.0	15018	14.65	128.7	126.5	43.8	8.59	5.45
100.0	1.00	2.7	39.0	106.2	144221	15.06	87.0	84.6	20.2	12.01	6.58

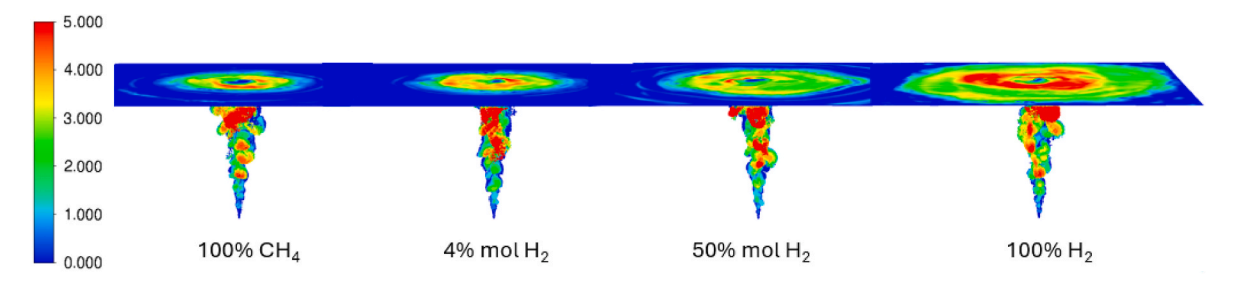


Fig. 6. Bubble plumes coloured by distance from plume axis and radial surface velocities coloured as indicated by colormap (m/s) for various gas blends 200 s after initiation of release.

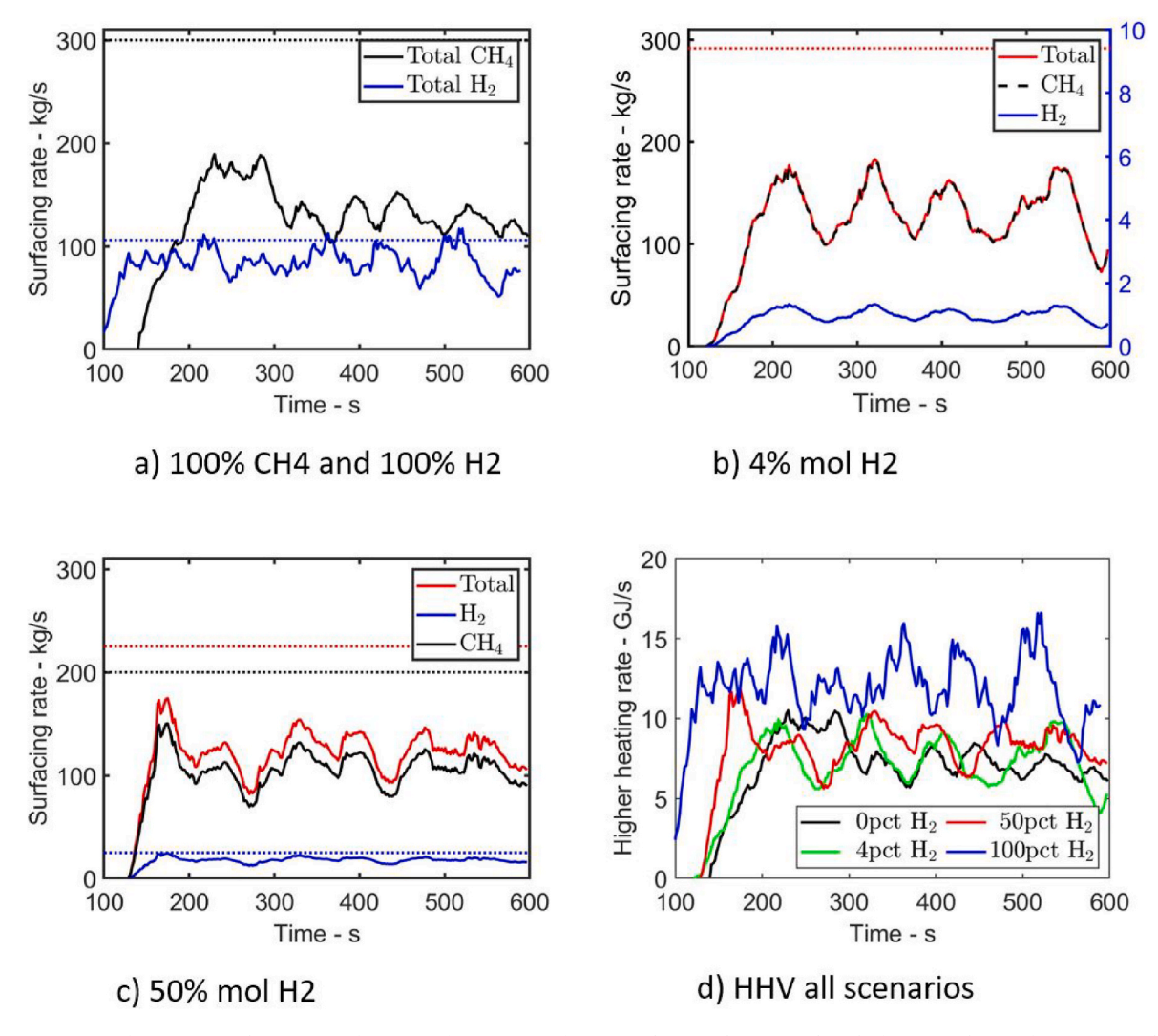


Fig. 7. Time varying surfacing rates and HHV. a) Surfacing rate for scenarios of 100 % mol CH<sub>4</sub> and 100 % mol H<sub>2</sub>, b) for 4 % mol H<sub>2</sub>, c) for 50 % H<sub>2</sub> and d) HHV for all scenarios. The dotted lines are the release rates.

given in Table 2 and the increase in surface velocities with increasing hydrogen content.

Fig. 8 shows 2D contour plots of the total surface flux and higher heating flux as distributed at the ocean surface. Even by averaging for 100 s, the flux does not represent a smooth curve consistent with the historical assumption of reporting this as a Gaussian profile. It is also seen that the surface flux decreases with increasing  $\rm H_2$  content in the released gas blend. Even if more of the  $\rm CH_4$  is dissolved in the ocean than  $\rm H_2$ , the effect of gas dissolution does not compensate for the reduced mass release rate associated with increasing  $\rm H_2$  content. A similar

comparison can be made for the higher heating flux as seen in Fig. 8 b). Here the higher heating value of  $H_2$  compared to  $CH_4$  causes the higher heating flux to increase with increasing  $H_2$  content even if the mass release rate decreases. This indicates that the risk related to gas concentrations in the atmosphere above the release increases as the  $H_2$  content of the gas blend increases.

# 3.1. Stripping of nitrogen and oxygen

The above assessments account for mass transfer of hydrogen and

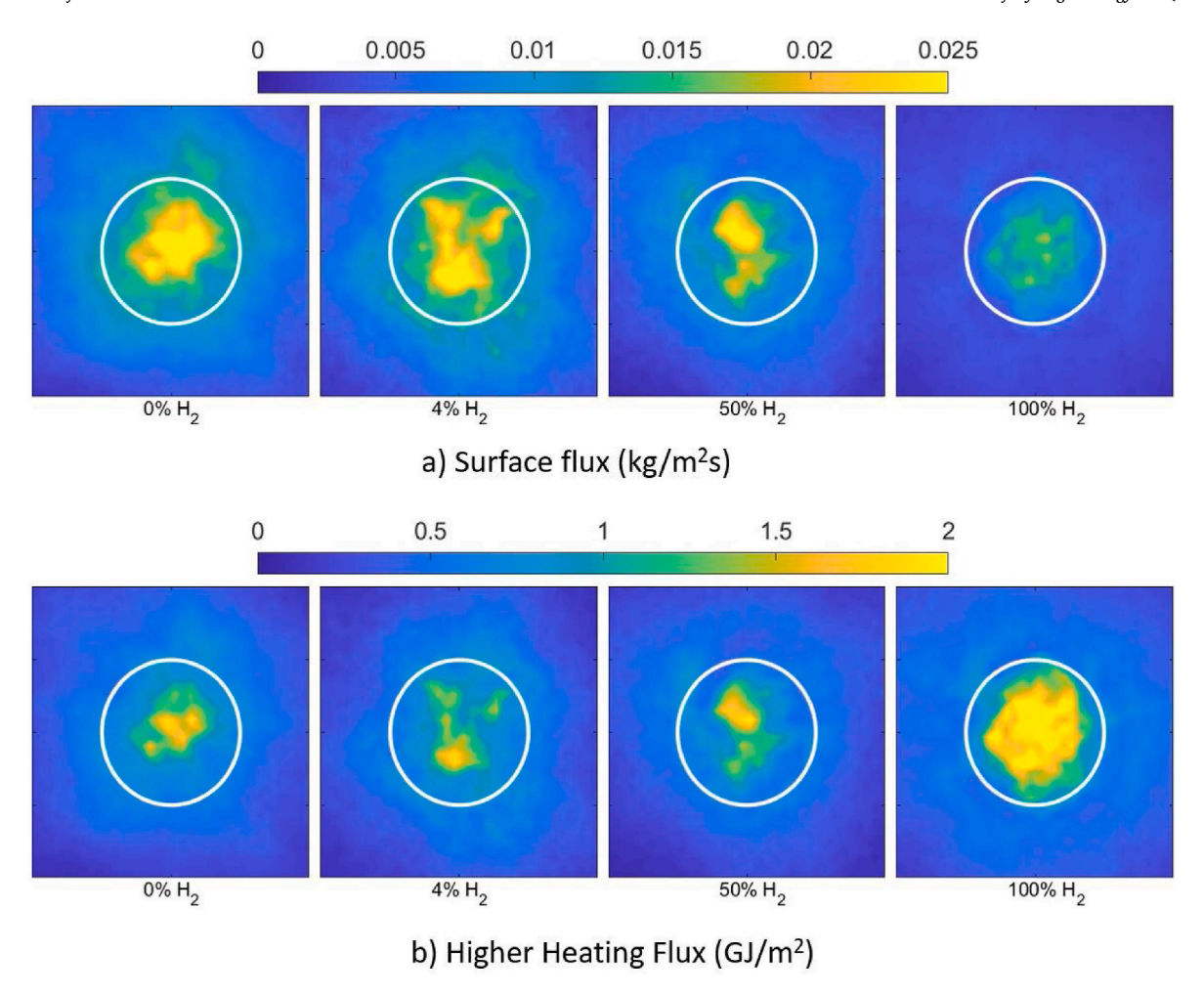


Fig. 8. Contour plots of total surface flux (a) and higher heating flux (b) averaged for 100 s for the analysed scenarios. Width and height of plots represents 200 m. The white circle has a radius of 50 m.

methane primarily as gas dissolution to the ocean. If the dissolved concentrations of the species accumulate to levels above the saturation limit, the mass transfer will be reversed, and the bubbles will receive gas as can be concluded by Eq. (3). This also implies that nitrogen and oxygen naturally occurring in the ocean will be transferred into the bubbles as they migrate upwards, sometimes referred to as stripping of dissolved gases.

In order to assess the impact of this, the scenario with 50 % mol H<sub>2</sub> was assessed by also accounting for stripping of nitrogen and oxygen. The concentration of these gases in the ocean will vary with season and geographical location. In this study we have assumed that their concentrations are given by equilibrium with the atmosphere (i.e. no biological effects and concentrations equivalent to the solubility at 1 atm and 5 °C) since more specific concentration profiles will only be valid for a given location at a given time. This gives a constant molar concentration of  $1.03 \cdot 10^{-5}$  for  $N_2$  and  $5.53 \cdot 10^{-6}$  for  $O_2$ . The driving force for stripping is higher closer to the surface since the pressure is lower and thus the solubility is lower. A scenario with similar conditions, but the release occurring at a depth of 500 m was also assessed. The analyses shows that the composition of the bubbles changes as they move upwards. Due to difference in solubility the composition of CH<sub>4</sub> decreases and H2 increases as bubbles move upwards. Closer to the ocean surface the stripping of N<sub>2</sub> and O<sub>2</sub> becomes more significant and starts affecting the overall composition of the bubbles. This is seen in Fig. 9 where the molar concentrations of the bubbles are plotted. The changes in the bubble composition are more significant for the scenario with a release from 500 m since the bubbles are exposed longer to mass transfer.

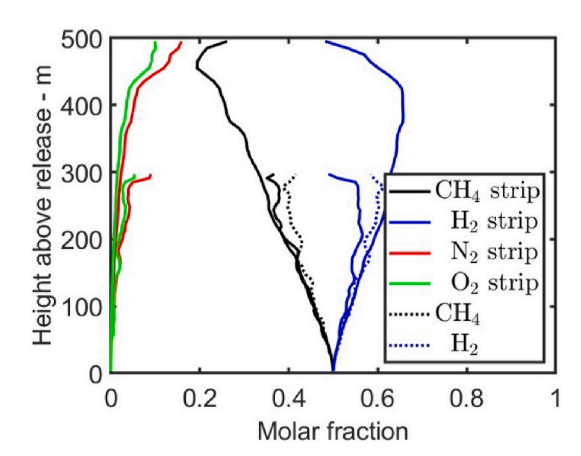


Fig. 9. Gas composition of bubbles as function of height above release for releases with and without stripping of  $N_2$  and  $O_2$  from 300 m and 500 m.

While the molar fraction of  $H_2$  increases significantly as the bubbles rise to the surface, the mass fraction is still relatively low. This implies that the surface flux of  $H_2$  is low compared to CH<sub>4</sub>. This is seen in Fig. 10 where the surface flux of the different gas components is seen. Note that the fluxes of the stripped  $N_2$  and  $O_2$  are in fact higher than that of  $H_2$ . This is primarily caused by the low density of  $H_2$ . The time averaged results seen in Table 3 document that roughly the same amount of CH<sub>4</sub> and  $H_2$  reaches the surface from 300 m whether stripping is accounted

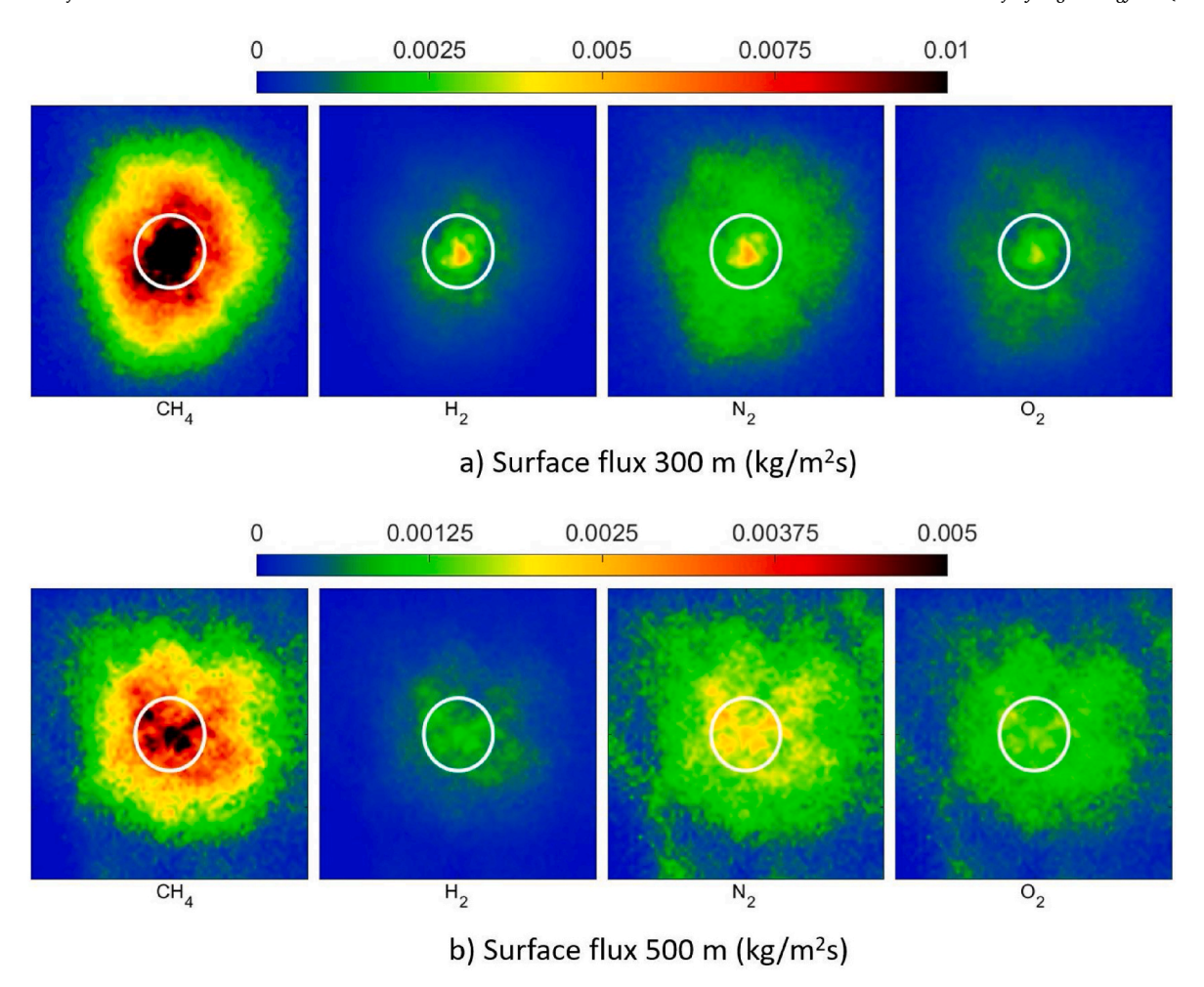


Fig. 10. Surface flux of the individual gas components averaged between 500 and 600 s after initiation of release from 300 m (a) and 500 m (b).

Table 3
Surfacing data on 225 kg/s release.

	Surfacing rate		HHV
	Total	CH <sub>4</sub> +H <sub>2</sub>	
	kg/s	kg/s	GJ/s
300 m, no strip	126.5	126.5	8.59
300 m, strip	205.5	131.1	8.86
500 m, strip	147.2	64.2	4.49

for or not. However, the total surfacing rate increases with stripping since also  $N_2$  and  $O_2$  is brought to the surface. From 500 m more of the released gas dissolves since the bubbles are exposed longer to mass transfer. The heating rate is also not directly affected by stripping of  $N_2$  and  $O_2$  since they have no contribution to the higher heating rate (heating value  $=\,$ 0). Thus, the averaged higher heating rate is quite similar for the release from 300 m both with and without accounting for stripping of  $N_2$  and  $O_2$ . The release scenario from 500 m has a lower higher heating rate since more of the released  $CH_4$  and  $H_2$  has been dissolved due to the longer residence time of bubbles in the ocean compared to the release from 300 m.

## 4. Conclusions

A transient 3-dimensional numerical model for analysing the fate of an underwater gas release from a damaged pipeline has been further developed to account for gas mixtures consisting of multiple gas components. The model is consistent with observations of single component  $CH_4$  releases. It has been applied to study release of hydrogen gas blends, i.e. hydrogen mixed with natural gas (here considered as pure methane). The model's outputs can inform emergency response planning by predicting gas surfacing locations and concentrations under varying leak scenarios.

Results show that the gas bubbles change its composition as they migrate upwards towards the ocean surface to contain relatively more hydrogen and less methane since methane is more soluble in water than hydrogen. The bubbles also strip the ocean for nitrogen and oxygen naturally occurring in the ocean and thus provide the bubbles with a nitrogen and oxygen content. Overall, the higher heating value reaching the ocean surface is less than the value released due to gas dissolution. When comparing scenarios with different hydrogen content, it is seen that a higher hydrogen content results in higher heating rates and higher hydrodynamic loads at the ocean surface when emanating from pipelines with the same operating conditions. The risk thus increases as the hydrogen content increases in the gas mixture. While other studies on underwater gas release also demonstrate capability to assess this risk [17,20,24,36] of various gas compositions (mostly air, methane or carbon dioxide), none of them have addressed underwater release hydrogen blends or underwater release of pure hydrogen from a depth where gas dissolution is significant.

While it can be argued that the risk correlates with the higher heating surfacing rate, the appropriate procedure to assess the risk is to export the calculated surface fluxes to a numerical simulation of the atmospheric dispersion of the gas components and then assess the atmospheric concentrations. This has not been the focus of this study. Other

future enhancements include performing release experiments with hydrogen and hydrogen blends at significant depths for gas dissolution and validating the numerical model against the observations. However, it should be noted that assessments of potential natural gas incidents have historically been based on models validated by experiments on air bubbles. More realistic gas densities should be implemented. With enhanced gas density and a validated model, a greater span of scenarios can be assessed to map the true extension of the risk potential. This includes shallower and deeper depths and more variations of release rates and blending ratios.

## CRediT authorship contribution statement

**J.E. Olsen:** Writing – original draft, Visualization, Methodology, Formal analysis, Conceptualization. **P. Skjetne:** Writing – review & editing, Methodology, Conceptualization.

## Declaration of competing interest

The authors declare that they have no known competing financial interests or personal relationships that could have appeared to influence the work reported in this paper.

## Acknowledgement

The work presented in this publication is carried out in the SHIMMER-project co-funded by the European Union (Project ID 101111888). Views and opinions expressed are however those of the authors and do not necessarily reflect those of the European Union or the Clean Hydrogen Joint Undertaking. Neither the European Union nor the Granting Authority can be held responsible for them. The project is supported by the Clean Hydrogen Partnership and its members.

#### References

- [1] Martin P, Ocko IB, Esquivel-Elizondo S, Kupers R, Cebon D, Baxter T, et al. A review of challenges with using the natural gas system for hydrogen. Energy Sci Eng 2024;12:3995–4009. https://doi.org/10.1002/ese3.1861.
- [2] Islam A, Alam T, Sheibley N, Edmonson K, Burns D, Hernandez M. Hydrogen blending in natural gas pipelines: a comprehensive review of material compatibility and safety considerations. Int J Hydrogen Energy 2024;93:1429–61. https://doi.org/10.1016/j.ijhydene.2024.10.384.
- [3] Alfasfos R, Sillman J, Soukka R. Lessons learned and recommendations from analysis of hydrogen incidents and accidents to support risk assessment for the hydrogen economy. Int J Hydrogen Energy 2024;60:1203–14. https://doi.org/ 10.1016/j.ijhydene.2024.02.226.
- [4] Perry RH, Green D. Perry's chemical engineers' handbook. sixth ed. Singapore: McGraw-Hill: 1984.
- [5] Taylor G. The action of a surface current used as a breakwater. ProcRoySocA 1955; 231. https://doi.org/10.1098/rspa.1955.0188.
- [6] Hunt GR, van den Bremer TS. Classical plume theory 1937-2010 and beyond. IMA J Appl Math 2011;76:424–48. https://doi.org/10.1093/imamat/hxq056.
- [7] Batchelor GK. Heat convection and buoyancy effects in fluids. Q J R Meteorol Soc 1954;80:339–58. https://doi.org/10.1002/qj.49708034504.
   [8] Evans JT. Pneumatic and similar breakwaters. ProcRoySocA 1955;231:457–66.
- [8] Evans JT. Pneumatic and similar breakwaters. ProcRoySocA 1955;231:457–66 https://doi.org/10.1098/rspa.1955.0187.
- [9] Morton BR, Taylor GI, Turner JS. Turbulent gravitational convection from maintained and instantaneous sources. ProcRoySocA 1956;234:171–8.
- [10] Ditmars JD, Cederwall K. Analysis of air-bubble plumes. 1974. p. 2209–26.
- [11] Topham DR. Hydrodynamics of an oil well blowout. Inst Ocean Sci 1975.
- [12] Fanneløp TK, Sjøen K. Hydrodynamics of underwater blowouts. Norweg Marit Res 1980;4:17–33.
- [13] Milgram JH. Mean flow in round bubble plumes. J Fluid Mech 1983;133:345–76. https://doi.org/10.1017/S0022112083001950.
- [14] Yapa PD, Zheng L. Simulation of oil spills from underwater accidents .1. model development. J Hydraul Res 1997;35:673–87.
- [15] Socolofsky SA, Adams EE. Multi-phase plumes in uniform and stratified crossflow. J Hydraul Res 2002;40:661–72. https://doi.org/10.1080/00221680209499913.
- [16] Johansen O. Development and verification of deep-water blowout models. Mar Pollut Bull 2003;47:360–8. https://doi.org/10.1016/S0025-326X(03)00202-9.
- [17] Dissanayake A, Gros J, Socolofsky SA. Integral models for bubble, droplet, and multiphase plume dynamics in stratification and crossflow. Environ Fluid Mech 2018;18:1167–202. https://doi.org/10.1007/s10652-018-9591-y.

- [18] Buscaglia GC, Bombardelli FA, García M. Numerical modeling of large-scale bubble plumes accounting for mass transfer effects. Int J Multiphas Flow 2002;28: 1763–85. https://doi.org/10.1016/S0301-9322(02)00075-7.
- [19] Cloete S, Olsen JE, Skjetne P. CFD modeling of plume and free surface behavior resulting from a sub-sea gas release. Appl Ocean Res 2009;31:220–5. https://doi. org/10.1016/j.apor.2009.09.005.
- [20] Li X, Han Z, Yang S, Chen G. Underwater gas release modeling and verification analysis. Process Saf Environ Prot 2020;137:8–14. https://doi.org/10.1016/j. psep.2020.02.011.
- [21] Engebretsen T, Northug T, Sjøen K, Fanneløp TK. Surface flow and gas dispersion from a subsea release of natural gas. International Society of Offshore and Polar Engineers; 1997. p. 566–73.
- [22] Olsen JE, Skjetne P. Summarizing an Eulerian-Lagrangian model for subsea gas release and comparing release of CO2 with CH4. Appl Math Model 2020;79: 672–84. https://doi.org/10.1016/j.apm.2019.10.057.
- [23] Fraga B, Stoesser T, Lai CCK, Socolofsky SA. A LES-Based Eulerian–Lagrangian approach to predict the dynamics of bubble plumes. Ocean Model 2016;97:27–36. https://doi.org/10.1016/j.ocemod.2015.11.005.
- [24] Li X, Wang Z, Chen G. Modeling underwater plumes of gas released from seafloor soil: a comparison of different gases. Process Saf Environ Prot 2024;184:950–60. https://doi.org/10.1016/j.psep.2024.02.014.
- [25] Cassano K, Pierro A, Froio G, Perini R, Farinelli P, De Marco G, et al. High-pressure gas release from subsea pipelines: multiphase modelling and CFD simulation for consequences analysis in risk assessment. J Loss Prev Process Ind 2023;81:104962. https://doi.org/10.1016/j.jlp.2022.104962.
- [26] Johansen O, Rye H, Cooper C. DeepSpill field study of a simulated oil and gas blowout in deep water. Spill Sci Technol Bull 2003;8:433–43. https://doi.org/ 10.1016/S1353-2561(02)00123-8.
- [27] Olsen JE, Skjetne P. Current understanding of subsea gas release a review. Can J Chem Eng 2016;94:209–19. https://doi.org/10.1002/cjce.22345.
- [28] Dissanayake Anusha L, Gros Jonas, Drews Henning Johannes, Nielsen Jacob Woge. Fate of methane from the nord stream pipeline leaks. Environ Sci Technol Lett 2023;10:903-8
- [29] Harris SJ, Schwietzke S, France JL, et al. Methane emissions from the nord stream subsea pipeline leaks. Nature 2025;637:1124–30. https://doi.org/10.1038/ s41586-024-08396-8.
- [30] Leifer I, Patro RK. The bubble mechanism for methane transport from the shallow sea bed to the surface: a review and sensitivity study. Cont Shelf Res 2002;22: 2409–28.
- [31] Olsen JE, Krause D, Davies EJ, Skjetne P. Observations of rising methane bubbles in trondheimsfjord and its implications to gas dissolution. J Geophys Res: Oceans 2019;124:1399–409. https://doi.org/10.1029/2018JC013978.
- [32] McGinnis DF, Greinert J, Artemov Y, Beaubien SE, Wüest A. Fate of rising methane bubbles in stratified waters: how much methane reaches the atmosphere? J Geophys Res 2006;111:2156–202. https://doi.org/10.1029/2005JC003183.
- [33] Rehder G, Leifer I, Brewer PG, Friedrich G, Peltzer ET. Controls on methane bubble dissolution inside and outside the hydrate stability field from open ocean field experiments and numerical modeling. Mar Chem 2009;114:19–30. https://doi. org/10.1016/j.marchem.2009.03.004.
- [34] Wang B, Socolofsky SA, Breier JA, Seewald JS. Observations of bubbles in natural seep flares at MC 118 and GC 600 using in situ quantitative imaging. J Geophys Res Oceans 2016:121:2203–30.
- [35] Olsen Jan Erik, Skjetne P. On the surfacing mechanism of bubble plumes from subsea gas release. In: Progress in applied CFD – CFD2017 selected papers from 12th international conference on computational fluid dynamics in the oil & gas, metallurgical and process industries. Trondheim: SINTEF akademisk forlag; 2017. p. 399–403.
- [36] Mercuri A, Blasioli G, Mauge R, Busini V, Fehervari M, Aloigi E, et al. Quantitative risk assessment of CO2 & H2 offshore pipelines - advancing on modelling subsea accidental releases. 2023. https://doi.org/10.4043/32603-MS. Houston.
- [37] Liu J, Huang D, Zhang X, Wang Z, Tsai Y, Pan Y. Research progress on leakage and diffusion of CH4 and H2/CH4 in buried and submarine pipeline transportation processes. Emergency Manag Sci Technol 2025;5. https://doi.org/10.48130/emst-0025-0007
- [38] Huser A, Bengherbia T, Olsen JE, Skjetne P. Subsea gas plumes and dispersion above sea. Safety, reliability and risk analysis. first ed. London: CRC Press; 2013.
- [39] Li X, Khan F, Yang M, Chen C, Chen G. Risk assessment of offshore fire accidents caused by subsea gas release. Appl Ocean Res 2021;115:102828. https://doi.org/ 10.1016/j.apor.2021.102828.
- [40] Ranz WE, Marshall WRJ. Evaporation from droplets, parts I & II. Chem Eng Prog 1952;48:173–80.
- [41] Wilke CR. A viscosity equation for gas mixtures. J Chem Phys 1950;18:517–9. https://doi.org/10.1063/1.1747673.
- [42] Huber M. The NIST REFPROP database for highly accurate properties of industrially important fluids. IndEngChem Res 2022;61:15449–72.
- [43] Lemmon E, Huber M, McLinden M. Nist reference fluid thermodynamic and transport properties database (refprop). 2007.
- [44] Wiesenburg DA, Guinasso NLJ. Equilibrium solubilities of methane, carbon monoxide, and hydrogen in water and seawater. J Chem Eng Data 1979;24.
- [45] Hamme RC, Emerson SE. The solubility of neon, nitrogen and argon in distilled water and seawater. Deep-Sea Res 2004;51:1517–28.

- [46] García HE, Gordon LI. Oxygen solubility in seawater: better fitting equations. Limnol Ocenaogr 1992;37:1307–12.
  [47] Hayduk W, Laudie H. Prediction of diffusion coefficients for nonelectrolytes in dilute aqueous solutions. AIChE J 1974;20:611–5.
- [48] Othmer DF, Thakar MS. Correlating diffusion coefficients in liquids. IndEngChem 1953;45:589.